First-principles study of the preference for zinc-blende or rocksalt structures in FeN and CoN

Pavel Lukashev and Walter R. L. Lambrecht
Department of Physics, Case Western Reserve University, Cleveland, Ohio 44106-7079, USA
(Received 18 May 2004; revised manuscript received 2 September 2004; published 8 December 2004)

The energies of zinc-blende and rocksalt structures FeN and CoN were calculated as function of lattice constant using the local density approximation and generalized gradient approximation density functional methods and the linear muffin-tin orbital band-structure method. The zinc-blende structure is found to be preferred in both cases at ambient pressure. The transition pressure for the zinc-blende to rocksalt phase transition is calculated to be about 50 and 30 GPa for FeN and CoN, respectively. Spin-polarized calculations indicate that rocksalt FeN has a small but nonzero magnetic moment near its equilibrium lattice constant, while CoN has zero magnetic moment below a certain critical value of the lattice constant. The magnetic moment increases abruptly near a certain critical lattice constant for both materials. The zinc-blende phases are found to be nonmagnetic. In FeN a ferromagnetic ordering is predicted but the energy difference with the antiferromagnetic AFM-I alignment is very small. Densities of states and band structures are given for both structures and used to discuss the structural preference and magnetic behavior.

DOI: 10.1103/PhysRevB.70.245205 PACS number(s): 71.20.Ps, 64.70.Kb, 75.50.Cc

I. INTRODUCTION

Most transition metal (TM) nitrides are well known to be refractory metals, characterized by high-hardness and high-temperature resistance.[1] Some of these compounds also have interesting magnetic properties—e.g., $[001]_1$ antiferromagnetic order in MnN[2] and AFM-$[110]_2$ in CrN.[3] This notation means spins are aligned in (110) planes but switch sign every other layer: $\uparrow\uparrow\downarrow\downarrow$. While most of the early TM nitrides have the rocksalt (RS) structure, it was recently reported that FeN and CoN films grown by reactive sputtering in a mixture of $Ar+N_2$ gas have the zinc-blende (ZB) structure.[4,5] In fact, in CoN, there has been some discussion in the earlier literature about the crystal structure and both ZB and RS structures have been reported depending on the synthesis method. Schmidt-Dumont and Kron[6] obtained rocksalt CoN with a lattice constant of 4.27 Å by decomposition of $Co(NH_2)_3$, while Taylor *et al.*[7] obtained zinc-blende CoN with a lattice constant of 4.28 Å by decomposing $[Co(NH_3)_6](N_3)_3$.

Earlier theoretical work on the electronic structure and cohesive energy in the 3*d* TM nitrides has focused on the rocksalt structure.[8,9] The purpose of the present paper is to study the relative energy difference of the ZB and RS structures for FeN and CoN, the possibility of a high-pressure phase transition between them, and their differences in electronic structure. The ZB structure of these transition-metal nitrides might make them attractive as Schottky barrier or Ohmic contact materials on semiconductors because it may facilitate epitaxial growth with high-quality sharp interfaces. The fairly small lattice constant limits the semiconductors that would match to it to GaN and SiC but these are important wide-band-gap semiconductors. Recently, there has been considerable interest in ferromagnetic compounds matched to semiconductors as possible sources of spin injection into semiconductors. From this point of view it is also interesting to investigate whether or not FeN and CoN exhibit magnetism.

Morita *et al.*[10] reported antiferromagnetism for FeN below 100 K, while Suzuki *et al.*[4] reported mictomagnetic behavior. This is evidenced by the observed dependence of the magnetization on whether the sample is cooled in the presence or absence of a magnetic field. In particular, they found a decrease of the magnetization with decreasing temperature in zero-field-cooled samples below a specific temperature T_s where the zero-field-cooled and field-cooled magnetizations start to differ. On the basis of these observations they suggested an antiferromagnetic matrix with a small amount of ferromagnetic impurities, possibly other phases of Fe_xN with higher Fe content, which are known to be ferromagnetic. In CoN,[5] only paramagnetic behavior was observed, with some residual effects of small amounts of ferromagnetic impurities, again attributed to higher Co content Co_xN phases. In this paper, we carried out spin density functional calculations in both the ZB and RS phases to investigate if any magnetic moments are formed.

II. COMPUTATIONAL METHOD

The theoretical framework of our calculations is the density functional method[11] in the local density approximation (LDA) and generalized gradient approximations (GGA). The random phase approximation (RPA) parametrization of Hedin and Lundqvuist[12] was used for exchange and correlation and combined with the Langreth-Mehl gradient correction.[13] For the spin-polarized case, the closely related von Barth–Hedin[14] parametrization is used for the local spin density approximation (LSDA).

Our calculations are carried out using the linear muffin-tin orbital band-structure method[15] (LMTO) in both the atomic sphere aproximation (ASA) and a recently developed full-potential (FP) implementation.[16] The ASA is expected to work well for these high-symmetry and close-packed structures. As usual, empty spheres are introduced in both the RS and ZB structures to make the sphere packing sufficiently close when doing the ASA calculations. They were not included in the FP-LMTO calculations. The FP-LMTO method provides an important check. The ASA was used mainly because it allowed us to check the effect of the GGA which was

not yet implemented in the present FP-LMTO code. The tetrahedron method is used for Brillouin zone integration with a well-converged set of **k**-points based on a regular division of the reciprocal unit cell in a $10\times10\times10$ mesh.

While the ASA LMTO method uses a "minimal" basis set of *spd* electrons on each site and the empty spheres, the FP-LMTO method was used with an enhanced basis set. Each basis orbital is characterized by a κ value and a smoothing radius, giving the overall decay and the behavior near the muffin-tin sphere, of the smoothed Hankel functions chosen as envelope functions. Inside the muffin-tin spheres, the envelope functions are augmented—i.e. matched in value and slope to a linear combination of $\phi_{\nu l}$ and $\dot{\phi}_{\nu l}$, the solutions to the spherical part of the potential and their energy derivative for angular momenta l from 0 to 2 and a chosen linearization energy $E_{\nu l}$ chosen in the center of gravity of the occupied partial density of states of each angular momentum channel. The basis set consists of two *sp* basis orbitals on the TM atom and one *d* orbital and a single *spd* orbital on the N with a standard optimized choice of smoothing radii and κ values. The other convergence parameter of the FP-LMTO method is the size of the real-space mesh used to represent the smooth part of the charge density, potential, and wave functions. The convergence of this mesh is tested as part of the code and chosen to be a $16\times16\times16$ division of the unit cell. The energies are converged to 1 μRy in the self-consistent procedure.

Our initial ASA calculations, which used equal sphere radii, lead to fairly large discrepancies in bulk modulus between ASA and FP, up to 25%. This problem, however, could be overcome by a more optimal choice of sphere radii. The calculations presented here use ratios of sphere radii determined as follows. Starting from the overlapped electrostatic Hartree potential of the atomic charge densities, the point along a line from an Fe to a nearest-neighbor N atom is determined where the potential reaches a maximum. This point is used to determine the ratio of touching sphere radii. Similarly the sizes of the empty spheres are determined. Subsequently the spheres are increased uniformly in size such that the sum of sphere volumes equals the volume of the unit cell. This leads to somewhat larger Fe and Co sphere radii relative to those of the N and empty spheres, close to what one expects from atomic radii. This construction minimizes the discontinuities in the potential involved in the ASA and therefore provides a better approximation to the true potential. Although in the FP-LMTO method the choice of sphere radii is less crucial, we also adopted the same procedure to determine the ratio of touching sphere radii. In FP-LMTO method the sphere sizes were kept fixed at the values corresponding to touching spheres for the smallest lattice constant considered.

To find the transition pressure between the zinc-blende and rocksalt crystal structures we plot the enthalpy $H(p)=E[V(p)]+pV(p)$, where $V(p)$ is the volume corresponding to a given external pressure p obtained from $p(V)=-dE(V)/dV$, as a function of pressure for both structures, and find the intersection point. The calculated $E(a)$ curves are fitted by a convenient analytic equation of state of the form[17]

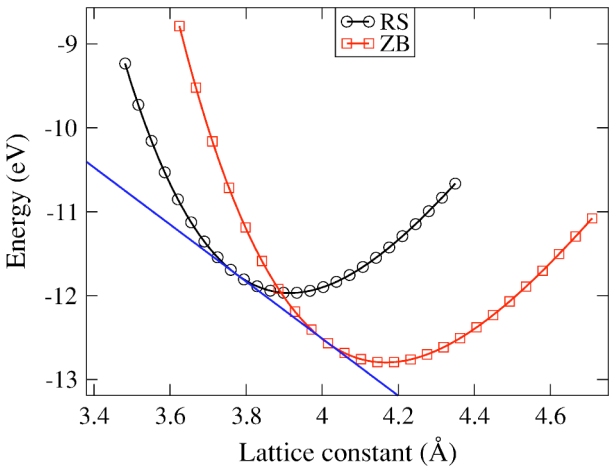

FIG. 1. (Color online) Energy vs lattice constant in FeN: non-spin-polarized, ASA-LDA.

$$E(a) = -E_c f[(a-a_0)/\ell], \tag{1}$$

in which E_c is the cohesive energy and $f(x)=e^{-x}(1+x+bx^3)$ is a universal binding energy form, with a_0 the equilibrium lattice constant and ℓ a length scale defined by $\ell=\sqrt{(4E_c/9a_0B)}$ in terms of the bulk modulus $B=-Vdp/dV$, from which the pressure and enthalpy are obtained analytically. From the fourth parameter in the fit b, which is related to the d^3E/da^3, we can obtain the pressure coefficient of the bulk modulus at equilibrium,

$$B' = 1+\frac{2}{3}\frac{a_0}{\ell}(1+3b). \tag{2}$$

III. RESULTS

A. Iron nitride

Figure 1 shows that the zinc-blende crystal structure for FeN has the lower energy minimum and that this minimum occurs at a larger lattice constant than for rocksalt. This means that at zero pressure, ZB is the preferred phase but at higher pressure, a phase transition to the RS phase may be possible. In fact, this would occur at the pressure where the enthalpies of the two phases are the same, corresponding to the common tangent construction, sketched in Fig. 1. As explained in Sec. II, we determine this transition pressure most accurately by plotting the enthalpies as shown in Fig. 2 and determine the intersection. This gives a transition pressure of 47 GPa. Slightly different values are obtained for this transition pressure when using the ASA-GGA (50 GPa) and FP-LDA (60 GPa) methods. We thus estimate the uncertainty to be ±10 GPa.

The results in Figs. 1 and 2 discussed so far were obtained in the ASA using the LDA, for non-spin-polarized calculations. Table I compares the equilibrium properties obtained with the different methods. First of all, we may note that all three approaches agree well on the lattice constant, the deviations being about 1% only. The ASA gives slightly lower values than the FP, and the LDA gives slightly lower values

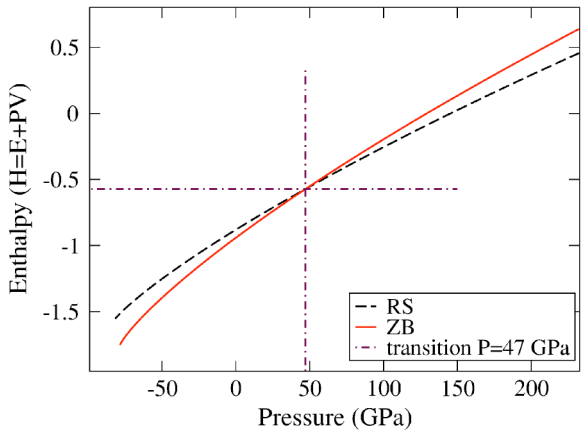

FIG. 2. (Color online) Enthalpy vs pressure in FeN: non-spin-polarized, ASA-LDA.

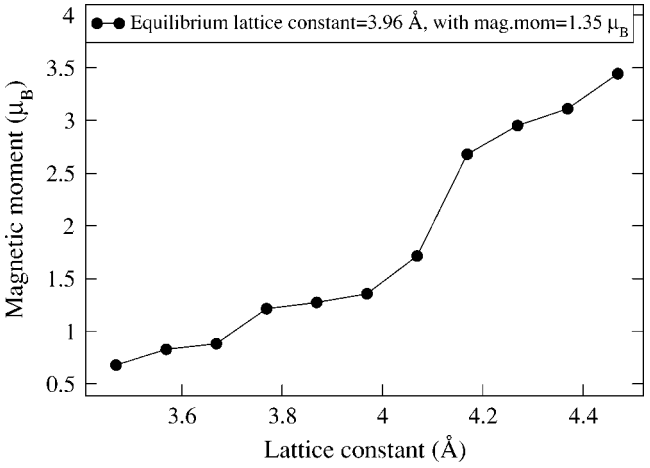

FIG. 3. Magnetic moment vs lattice constant in FeN, RS: ASA-LDA.

than the GGA. The cohesive energies are overestimated by the ASA compared to the FP and by the LDA compared to the GGA. This is a well-known feature of the GGA vs LDA approximations. The LDA has a tendency to overestimate the bonding. The improvement by the GGA is in fact mainly due to an improvement in the calculation of the atomic reference energies. Since the free atoms contain regions of very low density and strongly varying electronic density, gradient corrections to the exchange and correlation functional are more important for free atoms than for bulk. The lattice constant is usually underestimated with respect to the experimental lattice constant by up to a few percent by the LDA while the GGA sometimes overestimates it. Here, even the GGA seems to underestimate the lattice constant. However, we should keep in mind that the experimental lattice constant corresponds to that of a thin film, which may be influenced by the substrate and is not a true bulk value.

TABLE I. Equilibrium properties of FeN: lattice constant a, cohesive energy E_c per formula unit, bulk modulus B, and the pressure coefficient of bulk modulus B_0'.

	a (Å)	E_c (eV/cell)	B (GPa)	B_0'
ZB, non-spin-polarized				
ASA-LDA	4.169	13.3	322	4.2
ASA-GGA	4.195	11.2	308	4.3
FP-LDA	4.215	12.5	324	4.6
Expt.	4.307[a]	9.2[b]		
RS, spin-polarized				
ASA-LDA	3.960	12.4	316	5.6
ASA-GGA	4.021	10.3	248	5.8
FP-LDA	4.015	11.4	288	5.2
RS, non-spin-polarized				
ASA-LDA	3.937	12.3	395	4.5
ASA-GGA	3.967	10.1	370	4.5
FP-LDA	3.980	11.6	369	4.6

[a]Reference 4.
[b]Reference 8.

Turning to the bulk moduli, we first can see that the ASA and FP agree with each other to better than 10%, which is comparable to the usual error bar in this quantity compared to experimental values (not available for FeN to the best of our knowledge). The GGA is seen to decrease the bulk modulus compared to the LDA. The softening is again consistent with a weaker bonding. The decrease is strongest for the spin-polarized calculation of RS, of order 20%, whereas in the other cases it is only of order 5%. The B' value is also significantly increased in the spin-polarized case. We may note here that the corrections from the ASA to FP and from the LDA to GGA generally go in the same direction. This is in contrast with a discussion of GGA vs LDA errors for elemental transition metals by Ozoliņš and Körling,[18] but we note that this could sensitively depend on the choice of sphere radii in the ASA. It is not clear that GGA corrections and FP corrections can just be considered independent and additive because in the ASA treatment of the GGA terms only the spherically averaged contributions inside the spheres are included. Nevertheless, one may expect that the GGA values are closest to the experimental values and may still be a slight overestimate.

Turning now to spin-polarized calculations (using the FP-LMTO and LSDA) we find no magnetic moment in the ZB case, but a nonzero magnetic moment of $1.35\mu_B$ for the RS phase at its minimum-energy lattice constant. The magnetic moment as a function of lattice constant is shown in Fig. 3. It shows a striking nonlinear behavior with a rapid change near 4.126 Å—i.e., slightly above the minimum-energy lattice constant for RS. The higher magnetic moments for RS FeN at larger lattice constants than its equilibrium lattice constant indicate a more atomiclike behavior. In fact, the Fe-N bond distances are then pretty large and one may assume that this would weaken the Fe e_g-2Np bonds and thereby allow a greater spin polarization of the e_g states. This however is unrealistic because at these lattice constants, the system prefers the ZB crystal structure, in which there are fewer but stronger bonds. This covalency quenches the magnetism.

The total energy versus lattice constant in the nonmagnetic and spin-polarized cases are shown in Fig. 4. The total energy difference between the FM and nonmagnetic phase

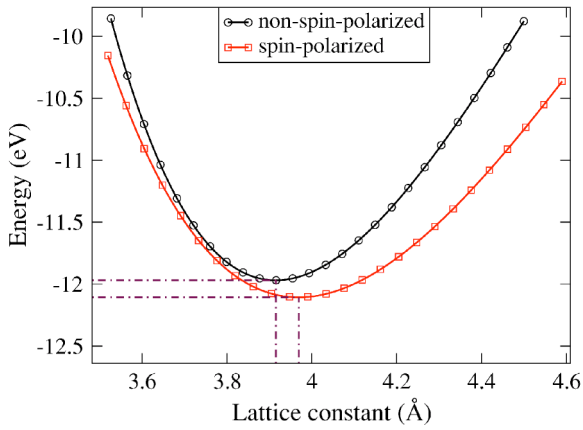

FIG. 4. (Color online) Energy vs lattice constant in nonmagnetic and spin-polarized cases for FeN, RS: ASA-LDA.

energy minima is 0.14 eV/unit cell. A slightly larger lattice constant is obtained for the spin-polarized case.

We also performed calculations for the AFM-I alignment of the magnetic moments. This corresponds to [001] layers of parallel spin within the layer but alternating spin direction between adjacent layers. We find that the energies for both configurations are very close to each other. The FM energy minimum is only 0.5 meV lower in energy than the AFM-I configuration and occurs at the same lattice constant 4.044 Å. This energy difference is too small to make a reliable conclusion on the nature of the magnetic ordering in the RS state. The energy difference $E_{AFM}-E_{FM}$ is shown as function of lattice constant in Fig. 5. Since the LSDA calculations usually underestimate the lattice constant slightly and the system prefers FM ordering for slightly larger lattice constant, we may expect that under pressure ZB FeN will first transform into a ferromagnetic RS structure. However, our calculations would predict a rather intriguing behavior. With further compression the system should convert to the AFM-I alignment and then back to the FM state. Although the energy differences considered here are quite small, we note that one may expect some cancellation of systematic errors in the absolute energies in taking the difference between two magnetic configurations. Clearly, there is a well-defined trend in the AFM-I and FM energy difference with lattice constant. On the other hand, it is hard to tell whether there really will be a range of lattice constants in which the AFM-I becomes the lower-energy configuration. If the whole curve shifts up slightly by a systematic error, the system would be predicted to be always ferromagnetic. Exploring this intriguing phase diagram experimentally would be rather challenging since pressures exceeding 50 GPa would be needed and magnetic measurements would have to be made on the samples while in a diamond anvil cell. Nevertheless, it is noteworthy from a theoretical point of view. At present we have no simple explanation for this behavior.

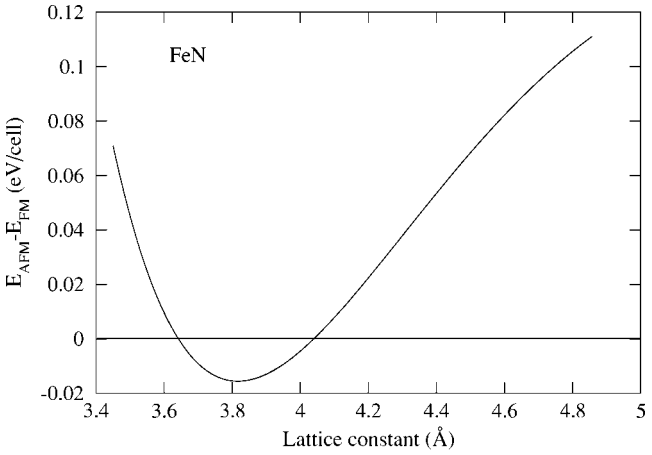

FIG. 5. Energy difference between AFM-I and FM configurations as a function of lattice constant in rocksalt FeN.

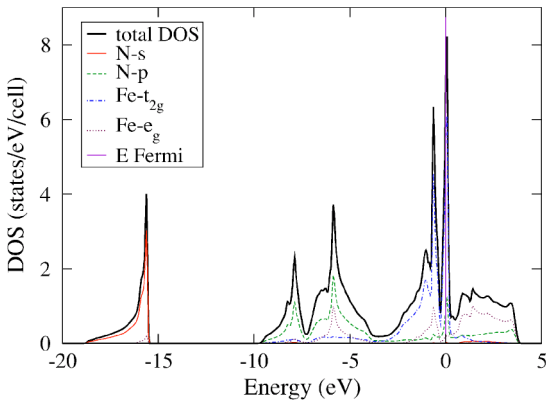

FIG. 6. (Color online) DOS and PDOS in FeN, RS, non-spin-polarized.

Density-of-states (DOS) plots are provided for both the spin-polarized and non-spin-polarized cases (see Figs. 6–8). They are resolved in partial DOS (PDOS) of N 2*p* and Fe 3*d* t_{2g} and e_g states in RS or t_2 and *e* states in ZB. Partial densities of states are defined by

$$N_{RL}(E) = \sum_{n\mathbf{k}} |\langle \phi_{RL}(E_{n\mathbf{k}}) | \psi_{n\mathbf{k}} \rangle|^2 \delta(E - E_{n\mathbf{k}}), \qquad (3)$$

where $\phi_{RL}(E) = \phi_{RL\nu} + (E - E_{RL\nu})\dot{\phi}_{RL\nu}$ is the partial wave of angular momentum $L=(l,m)$ in the muffin-tin sphere at

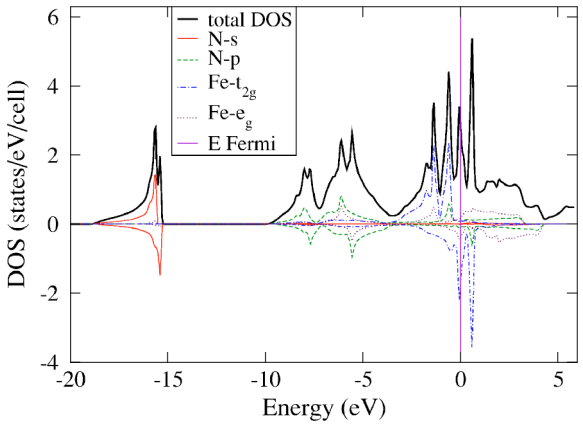

FIG. 7. (Color online) DOS and PDOS in FeN, RS, spin-polarized.

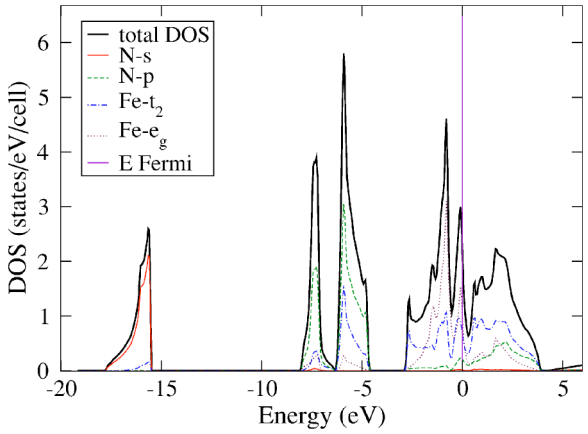

FIG. 8. (Color online) DOS and PDOS in FeN, ZB, non-spin-polarized.

atomic site R at the chosen energy, and $\psi_{n\mathbf{k}}$ is the nth eigenstate at the k point $\mathbf{k}$. The Brillouin zone integral is performed using the tetrahedron method. (Since the point group in ZB is T_d and lacks the inversion compared to O_h, the symmetry label does not include g referring to "gerade" or even states.) The DOS in ZB (Fig. 8) shows that the Fermi level lies at the lower edge of a "pseudogap," while in RS the Fermi level lies at a strong peak in the DOS. Using the Stoner exchange parameter I_S for Fe from Janak[19] of 0.46 eV and the DOS at the Fermi level for a single spin $\tilde{N}(E_F)$ $=3.45$ states/eV/Fe atom in RS and 1.05 states/eV/cell in ZB, respectively, we can see that the Stoner criterion $I_S\tilde{N}(E_F)>1$ is fullfilled for RS but not for ZB. Thus, the magnetic behavior of RS and nonmagnetic behavior of ZB is consistent with the Stoner theory. One can clearly see in Fig. 7 that the spin-up t_{2g} states move below the Fermi level while the spin-down states move partially above the Fermi level. The splitting is, however, not very large so that the net magnetic moment is fairly small. In fact, in a simple model one may assume that in this trivalent compound the two 4s and one of the 3d electrons of the atomic Fe $3d^64s^2$ configuration participate in the bonding, so that five electrons remain in the nonbonding t_{2g} states. This would give rise to a magnetic moment of $1\mu_B$. Since the e_g electrons are also partially spin polarized, the actual magnetic moment is somewhat larger.

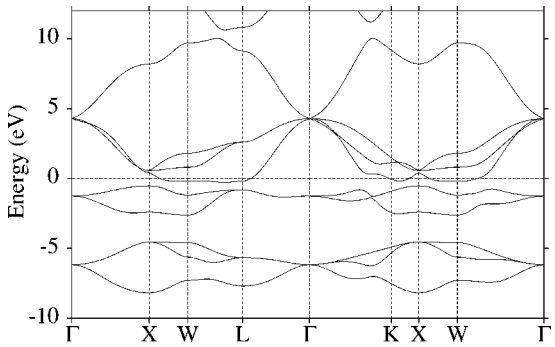

FIG. 9. Band structure of FeN, ZB, non-spin-polarized: ASA-LDA.

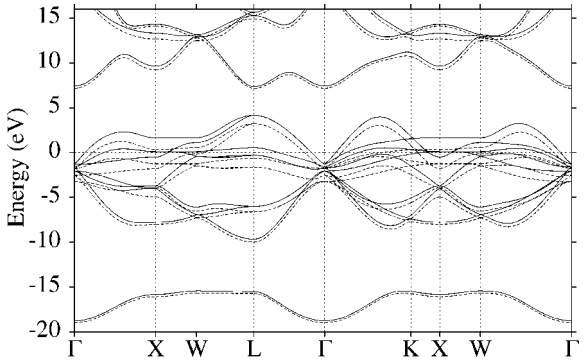

FIG. 10. Band structure of FeN, RS, spin-polarized: ASA-LDA. Solid lines: minority spin. Dashed lines: majority spin.

On the other hand, the location of the Fermi level in or near a pseudogap contributes to the stability of the ZB phase. One may notice that the relative ordering of the t_2 and e states is reversed in ZB and RS. As is well known, the t_2 lie lower than the e in octahedral environment (RS) and vice versa in tetrahedral environment (ZB). In the RS, however the e_g states form strong σ bonds with the N 2p states which lie in the range -3 to -9 eV while the corresponding antibonding states lie above the Fermi level. The t_{2g} states are nonbonding and give rise to the high peaks near the Fermi level. In ZB, the separation of t_2 and e states is not as clearly defined. For instance, both e and t_2 states contribute to the DOS from the Fermi level to about -3 eV below the Fermi level. The t_2 now form the predominant bonds with the N 2p states, giving rise to the two sharp peaks between -5 and -8 eV. These bands are much narrower than in the RS case because of the lower nearest neighbor coordination.

The band structures are shown for both zinc-blende and rocksalt structures in Figs. 9 and 10, respectively. These plots confirm the narrow N2p-Fet_2 bonding bands in ZB. For the RS we see a much stronger hybridization of the N2p and Fe3d bands, with small splitting of spin-up and spin-down states. Several bands are seen to cross the Fermi level, which will lead to a complex Fermi surface.

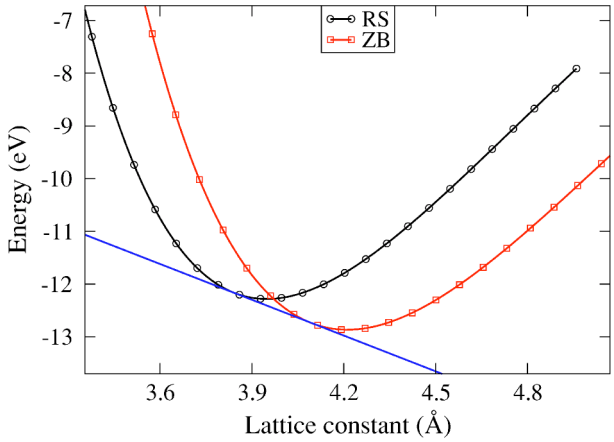

FIG. 11. (Color online) Energy vs lattice constant in CoN: non-spin-polarized, ASA-LDA.

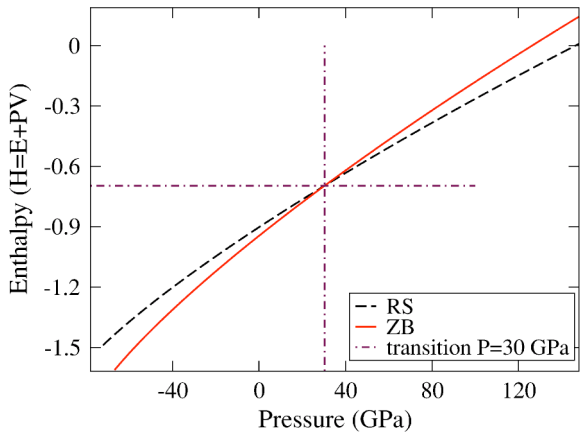

FIG. 12. (Color online) Enthalpy vs pressure, CoN: non-spin-polarized, ASA-LDA.

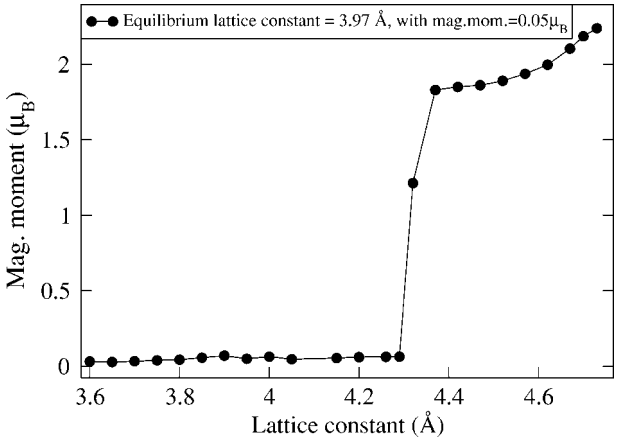

FIG. 13. Magnetic moment as a function of lattice constant in RS CoN.

B. Cobalt nitride

Very similar structural results are obtained for CoN as for FeN. Figure 11 shows that ZB has lower energy compared with RS; thus, ZB is the equilibrium structure at zero pressure.

A phase transition between ZB and RS is again predicted by plotting energy versus lattice constant and enthalpy versus pressure. The common tangent is shown in Fig. 11, and the enthalpy as function of pressure is shown in Fig. 12. Both indicate a phase transition from ZB to RS under pressure of about 30 GPa. Using the ASA-GGA and FP-LDA we obtain $p_t = 31$ GPa and 36 GPa, respectively.

The equilibrium lattice constant was determined for both the zinc-blende and rocksalt cases. For ZB it is 4.276 Å, and for RS it is 3.972 Å for FP-LMTO in LDA. This is to be compared with experimental result of 4.297 Å for ZB reported in Ref. 5. In Table II we summarize our results for the lattice constant, cohesive energy, bulk modulus, and pressure coefficient of the bulk modulus B_0' for CoN in the ZB and RS structures. The same trends in the GGA-LDA and FP-ASA comparisons hold as discussed earlier for FeN.

TABLE II. Equilibrium properties of CoN: lattice constant a, cohesive energy E_c per formula unit, bulk modulus B, and the pressure coefficient of bulk modulus B_0'.

	a (Å)	E_c (eV/cell)	B (GPa)	B_0'
	ZB, non-spin-polarized			
ASA-LDA	4.182	13.5	302	4.4
ASA-GGA	4.215	11.4	283	4.4
FP-LDA	4.276	12.9	294	4.9
Expt.	4.297[a]	9.1[b]		
	RS, non-spin-polarized			
ASA-LDA	3.932	12.8	378	4.6
ASA-GGA	3.964	10.7	350	4.7
FP-LDA	3.972	12.2	352	4.6

[a]Reference 5.
[b]Reference 8.

Only a negligibly small magnetic moment of $0.05\mu_B$ was detected for RS at its equilibrium lattice constant and no magnetic moment at all for ZB. Thus we conclude that CoN is essentially a nonmagnetic compound in agreement with experimental data.[5] However, as a function of lattice constant, we note that under expansion the RS of CoN does acquire a magnetic moment. The magnetic moment as a function of lattice constant in the RS structure is shown in Fig. 13.

Density of states (Figs. 14 and 15) and band structure (Figs. 16 and 17) plots are provided for both ZB and RS structures. We now have a fairly low DOS at the Fermi level for both ZB and RS. The Stoner parameter given by Janak[19] for Co is 0.49 eV. The DOS at the Fermi level for a single spin are 0.82 states/eV/cell in ZB and 1.48 states/eV/cell in RS, respectively. Thus, the Stoner criterion is not fulfilled for either of the two structures in agreement with the nonmagnetic nature of these compounds. The additional electron in Co compared to Fe has basically shifted the Fermi level slightly higher, so that it now lies almost in a pseudogap for RS. For ZB it no longer lies in the pseudogap but still lies in a low-DOS region. In the simple picture we discussed before for FeN, we now have the t_{2g} states completely filled, so no net magnetic moment is expected.

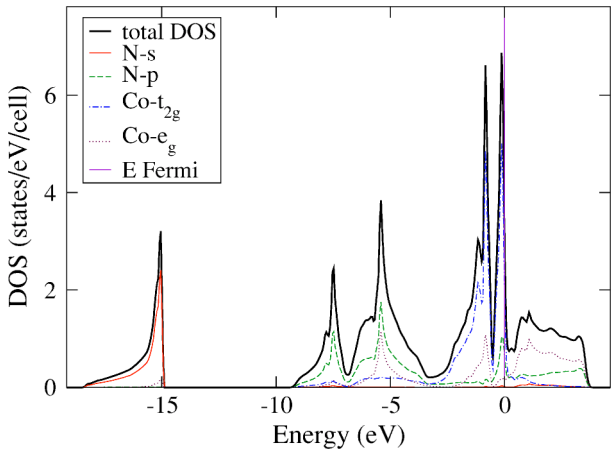

FIG. 14. (Color online) DOS and PDOS in rocksalt structure, CoN: non-spin-polarized.

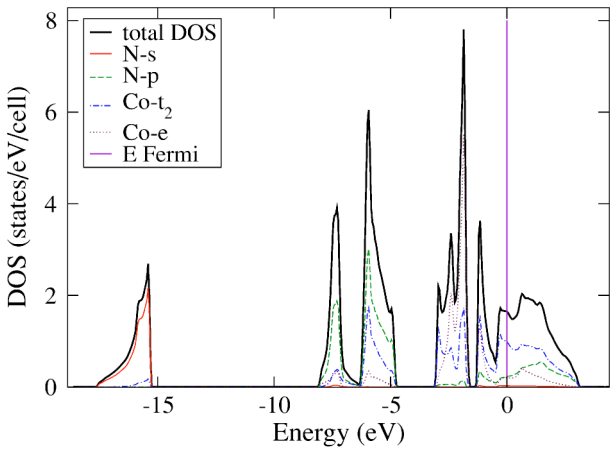

FIG. 15. (Color online) DOS and PDOS in zinc-blende structure, CoN: non-spin-polarized.

The discussion of the relative stability of ZB and RS in terms of the DOS is similar to that in FeN. In fact, one can see that essentially a rigid band picture holds. The bands and DOS are almost equal in both compounds, their only difference being the band filling which further reduces the tendency towards magnetism.

IV. DISCUSSION

Our computational results confirm the experimental results of Suzuki *et al.*[4,5] of the preference for the zinc-blende structure at atmospheric pressure. To the best of our knowledge, no high-pressure studies have yet been made of FeN or CoN so that our results for the phase transition are predictions remaining to be confirmed. However, our calculations show no indications of magnetism in the ZB phase, neither ferromagnetism nor antiferromagnetism. This indicates that the observed mictomagnetism in FeN is due to separate phases, but the reported antiferromagnetism of FeN at low temperature is in disagreement with our calculations. This claim of antiferromagnetism, however, was also based on rather indirect data because it is masked by the slight ferromagnetism of impurity phases and may need further study. Our calculations confirm an even less tendency towards magnetism in CoN which is explained simply by band filling in a rigid band picture. Unfortunately, this means that these

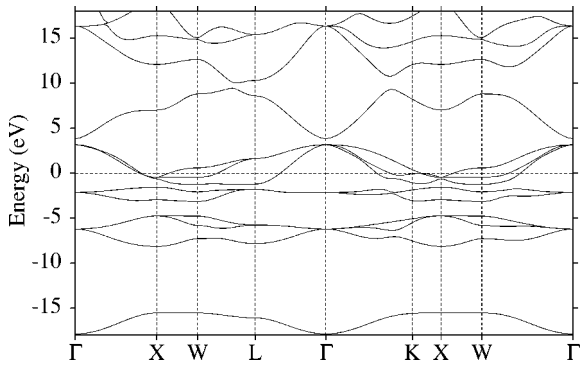

FIG. 16. Band structure of CoN, ZB, non-spin-polarized: ASA-LDA.

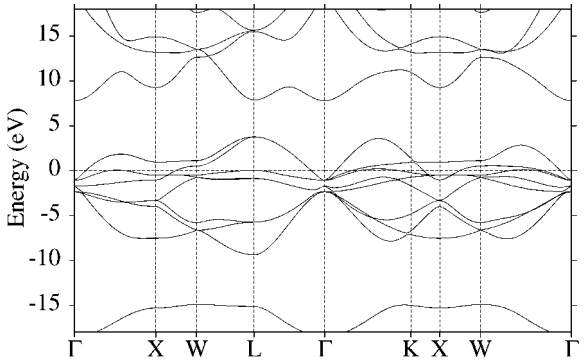

FIG. 17. Band structure of CoN, RS, non-spin-polarized: ASA-LDA.

materials are not as promising for spin injection as we had hoped. However, the fact that higher-TM-content compounds like Fe_4N do exhibit ferromagnetism and may occur as impurity phases in FeN may still allow for such applications. We would then need to consider the spin polarization of currents at both the Fe_4N/FeN and FeN/semiconductor interfaces. In some sense the ZB-FeN then would play the role of changing the conductivity and structure gradually between the ferromagnet and semiconductor. As is well known, the major problem in spin injection from a metallic ferromagnet to a semiconductor arises from their mismatch in impedance (or conductivity).[20] The ZB lattice structure would allow for a nice match to semiconductors such as GaN and SiC if the lattice constant of FeN and CoN can be slightly increased by doping with suitable atoms with larger atomic radii. This will be the subject of future work.

V. CONCLUSION

In this paper we have studied the crystal structure preference for zinc-blende or rocksalt structure, and the possible phase transitions between them, and the magnetic properties of iron nitride and cobalt nitride. The atmospheric pressure equilibrium crystal structure of both compounds was shown to be zinc-blende structure, in agreement with experimental results.[4,5] Zero magnetic moment was determined for zinc-blende structure of CoN and FeN, while the FeN was shown to possess a nonzero magnetic moment ($1.35\mu_B$) in the RS structure. The magnetic behavior was shown to be in agreement with the predictions of the Stoner theory. The transition pressures for the phase transition to the rocksalt were determined to be about 30 ± 5 and 50 ± 10 GPa for CoN and FeN, respectively. Rather interesting nonlinear behavior as a function of lattice constant was found for RS FeN both in terms of the magnitude of magnetic moment and in terms of the preference for FM or AFM ordering. Unfortunately, confirmation of these predictions by experiments is expected to be rather challenging because these will only occur under high pressure.

ACKNOWLEDGMENTS

This work was funded by the Office of Naval Research under Grant No. N00014-02-1-0880 and by the National Science Foundation under Grant No. ECS-0223634.

[1] A. Neckel, Int. J. Quantum Chem. **23**, 1317 (1983).
[2] A. Leineweber, R. Niewa, H. Jacobs, and W. Kockelmann, J. Mater. Chem. **10**, 2827 (2000).
[3] L. M. Corliss, N. Elliott, and J. M. Hastings, Phys. Rev. **117**, 929 (1960).
[4] K. Suzuki, H. Morita, T. Kaneko, H. Yoshida, and H. Fujimori, J. Alloys Compd. **201**, 11 (1993).
[5] K. Suzuki, T. Kaneko, H. Yoshida, H. Morita, and H. J. Fujimori, J. Alloys Compd. **224**, 232 (1995).
[6] O. Schmidt-Dumont and N. Kron, Angew. Chem. **67**, 231 (1955).
[7] B. Taylor, B. Joyner, and F. H. Verhoek, J. Am. Chem. Soc. **83**, 1069 (1961).
[8] J. Häglund, G. Grimvall, T. Jarlborg, and A. F. Guillermet, Phys. Rev. B **43**, 14 400 (1991).
[9] V. P. Zhukov, V. A. Gubanov, O. Jepsen, N. E. Christensen, and O. K. Andersen, Philos. Mag. B **58**, 139 (1988).
[10] H. Morita, H. Yoshida, T. Kaneko, H. Fujimori, and K. Suzuki, in *Proceedings of the 2nd International Symposium on the Physics of Magnetic Materials, Beijing 1992*, edited by S. Zhang (International Academic, Beijing, 1992), p. 633.
[11] P. Hohenberg and W. Kohn, Phys. Rev. **136**, B864 (1964); W. Kohn and L. J. Sham, Phys. Rev. **140**, A1133 (1965).
[12] L. Hedin and B. I. Lundqvist, J. Phys. C **4**, 2064 (1971).
[13] D. C. Langreth and M. J. Mehl, Phys. Rev. B **28**, 1809 (1983).
[14] U. von Barth and L. Hedin, J. Phys. C **5**, 2064 (1972).
[15] O. K. Andersen, Phys. Rev. B **12**, 3060 (1972); O. K. Andersen, T. Saha-Dasgupta, R. W. Tank, C. Arcangeli, O. Jepsen, and G. Krier, in *Electronic Structure and Physical Properties of Solids, The Uses of the LMTO Method*, edited by H. Dreyssé, Lecture Notes in Physics (Springer, Berlin, 2000), p. 3.
[16] M. Methfessel, M. van Schilfgaarde, and R. A. Casali, in *Electronic Structure and Physical Properties of Solids, The Uses of the LMTO Method*, edited by H. Dreyssé, Lecture Notes in Physics (Springer, Berlin, 2000), p. 114.
[17] J. H. Rose, J. R. Smith, F. Guinea, and J. Ferrante, Phys. Rev. B **29**, 2963 (1984).
[18] V. Ozoliņš and M. Körling, Phys. Rev. B **48**, 18 304 (1993).
[19] J. F. Janak, Phys. Rev. B **16**, 255 (1977).
[20] G. Schmidt, D. Ferrand, L. W. Molenkamp, A. T. Filip, and B. J. van Wees, Phys. Rev. B **62**, R4790 (2000).